SELF-ASSEMBLED STRUCTURES AND NANOASSEMBLIES

Synthesis of Palladium Nanoparticles on the Surface of Cerium(IV) Oxide under the Action of Ultraviolet Radiation and Their Characterization

M. V. Kirichkov[a],*, V. A. Polyakov[a,b],**, A. A. Tereshchenko[a],***, V. V. Shapovalov[a],****, A. A. Guda[a],*****, and A. V. Soldatov[a],******

[a] *Smart Materials Research Institute, Southern Federal University, Rostov-on-Don, 344090 Russia*
[b] *Southern Scientific Center, Russian Academy of Sciences, Rostov-on-Don, 344006 Russia*
*e-mail: mikhail.kirichkov@gmail.com
**e-mail: v.polakov93@gmail.com
***e-mail: antereshenko@sfedu.ru
****e-mail: vikt.shapovalov@gmail.com
*****e-mail: guda_sasha@mail.ru
******e-mail: soldatov@sfedu.ru
Received December 3, 2019; revised January 21, 2020; accepted January 26, 2020

Abstract—Palladium nanoparticles have been synthesized in an aqueous medium by ultraviolet irradiation using complex palladium oxalate as a precursor. The samples were studied by various laboratory methods, including transmission electron microscopy, X-ray fluorescence analysis, X-ray powder diffraction, X-ray absorption fine structure spectroscopy, and diffuse reflectance infrared spectroscopy with the use of CO probe molecules. The microimages obtained by transmission electron microscopy did not allow us to distinguish Pd nanoparticles from the material of the substrate but do not show any effect of ultraviolet irradiation on the sizes of CeO_2 nanoparticles. The X-ray fluorescence analysis data show the presence of cerium and palladium atoms in the material. X-ray diffraction patterns indicate the presence of phases of cerium dioxide and metallic palladium, while the analysis of the X-ray absorption fine structure spectra beyond the K-edge of palladium shows the presence of the PdO phase in the system. The approximate size of the palladium nanoparticles was estimated by the infrared spectra after the adsorption of CO and is less than 2 nm, which is significantly smaller than the average size of Pd nanoparticles obtained by a similar method without a CeO_2 substrate (1.5–9.5 nm).

INTRODUCTION

Due to their relatively high stability and wide range of applications, nanoparticles of precious metals attract increasing attention of researchers. In particular, they are used as hydrogen sensors [1], automotive catalysts [2], and catalysts for the hydrogenation and isomerization of olefins [3], as well as for fine organic synthesis, e.g., in Suzuki reactions [4] and Stille cross-coupling [5].

The efficiency of a catalyst directly depends on the degree of its dispersity and presence of active catalytic sites because the higher the dispersity is the larger the surface area is that is accessible for catalytic reactions. The material of the substrate onto which a nanomaterial is applied also plays a great role. There are many methods for the synthesis of palladium nanoparticles, the best known of which are codeposition [6–8] and impregnation [9, 10]. Polyol [11, 12] and microemul-sion [13, 7] syntheses, the method of reduction in a hydrogen flow [14], and the less common method of flame pyrolysis [15, 16] have also been described. However, not all of these methods make it possible to obtain nanoparticles with controlled sizes. Several different procedures for the preparation of ultrasmall nanoparticles of precious metals on various matrices have been described. They include the methods of modification of the surface of the substrate (in situ modification [17], postmodification [18, 19]). The efficiency of the modification of the surface is explained by the increase in the affinity of the precursor salt to the modified surface and, hence, a more uniform distribution of the growth centers of the nanoparticle nuclei on the surface of the matrix. However, despite their efficiency, such methods are multistage (which inevitably results in the loss of material at each of the stages), require high temperatures (solvothermal synthesis) and highly toxic reducing agents, as

well as being sensitive to the slightest changes in the external conditions, and they often require complex equipment for the synthesis.

One quite new and effective method for the synthesis of ultrasmall nanoparticles of precious metals is ultraviolet (UV) irradiation of their precursor salts. The major advantages of this method are its relative simplicity, high rate of reduction, and environmental friendliness. Thus-synthesized nanoparticles are subjected to agglomeration to a lesser extent, which excludes the need for introducing various surface-active substances and toxic solvents into the system as opposed to the standard procedures. Due to the relatively high value of the electrode potential of the Pd^{2+}/Pd^0 pair, as well as its low photostability, complex palladium salts are quite readily reduced and the selection of the optimum salt and radiation power makes it possible to complete the process within only minutes. Thus, the photoactivity of the salts can differ depending on the ligand environment that is used in extreme UV lithography [20]. Several procedures for UV reduction of the precursors of precious metals have been published. The influence of photoenergy at different wavelengths on the mechanisms of reduction of precious metal ions was presented in [21, 22]. The authors of [23] synthesized palladium nanoparticles with an average size of ~16 nm via UV treatment of an aqueous solution of complex palladium(II) oxalate. In [24], the synthesis of ultrasmall (2−3 nm) Pd nanoparticles deposited onto nanorods of gadolinium(III) hydroxide was described. In this case, gadolinium hydroxide acts as a photosensitizer, which made it possible to facilitate the decomposition of the less photoactive tetrachloropalladate(II). The synthesis of atomically dispersed palladium particles on a titanium dioxide matrix as catalysts for the hydrogenation of styrene and oxidation of carbon monoxide was reported in [25]. Similar results were published in [26]. The authors of [27] obtained bimetallic FePd nanoparticles with a size of approximately 7 nm on the surface of graphene layers. Palladium nanoparticles applied on a $NH_2-MIL-125$ metal organic framework were successfully used for the catalytic decomposition of a borane−ammonia complex [28]. Palladium nanoclusters with a size of approximately 3 nm on a SnO_2 substrate were also synthesized by photodeposition [29]. The authors of [30] obtained ultrasmall Pd nanoparticles on cerium dioxide nanofibers as a catalyst for the oxidation of carbon monoxide by water vapors. However, the method proposed by the authors is complex and multistage, as well as requiring toxic organic solvents and surface-active substances.

This work describes the synthesis and further characterization of palladium nanoparticles on cerium dioxide (Pd/CeO_2) obtained by the UV irradiation of an aqueous dispersion of CeO_2 containing a complex $[Pd(C_2O_4)_2]^{2-}$ as one of the most photoactive precursors that are free from highly toxic surface-active substances. Cerium dioxide was synthesized by a simple one-stage method and chosen due to its high thermal stability and relative chemical inertness, as well as its high oxygen storage capacity determined by the formation of a Ce^{4+}/Ce^{3+} oxidation−reduction pair that allows CeO_2 to effectively release catalytically active forms of oxygen.

MATERIALS AND METHODS

All the used chemicals were purchased from Sigma-Aldrich and were of analytical grade. To synthesize a CeO_2 substrate, 5 g of cerium(III) nitrate hexahydrate was dissolved in 240 mL of water under heating to 50°C and vigorous stirring. A 37% solution of ammonia was then added to the solution to pH of 9−9.5. Here, a brown precipitate was formed that gradually changed its color to violet due to the oxidation of the Ce^{3+} ions to Ce^{4+} ions. The obtained suspension was stirred overnight; as a result of this its color changed from violet to white, which indicated full oxidation of Ce^{3+} ions and formation of CeO_2. The precipitate was separated by centrifugation (5000 rpm, 10 min) and rinsed three times with distilled water. The obtained powder was calcinated at 600°C for 24 h.

To synthesize palladium nanoparticles supported on the surface of CeO_2, 20 mL of an aqueous solution of $PdCl_2$ (17.7 mg $PdCl_2$, 5 mmol/L) and 20 mL of an aqueous solution of $Na_2C_2O_4$ (67 mg $Na_2C_2O_4$, 25 mmol/L) were mixed by gradual pouring of an aqueous solution of $PdCl_2$ to a solution of $Na_2C_2O_4$ under vigorous stirring. The formation of a pale brown precipitate of palladium(II) oxalate was observed in the process of pouring. The obtained suspension was stirred for 20 min at 80°C. The precipitate gradually dissolved and the solution turned yellow−brown, which indicated the formation of a complex oxalate with the composition $Na_2[Pd(C_2O_4)_2]$ [31]. Next, 254 mg of CeO_2 was added to the obtained solution under vigorous stirring and heated at 80°C for 30 min. The obtained suspension was placed into a quartz crucible and treated by ultraviolet (UV) radiation for 30 min under vigorous stirring. The dispersion turned black−brown after irradiation. After cooling, the dispersion was divided to two fractions, namely, a black−brown precipitate and a black colloidal solution. The obtained fractions were washed with distilled water three times by centrifugation, the heavier fraction at 5000 rpm for 5 min and the colloidal solution at 10 000 rpm for 10 min, and then dried at 60°C for 1 d. The first fraction (the precipitate) was labeled DOWN, and the second (the colloidal solution), UP (Fig. 1).

Characterization by X-ray fluorescence analysis (XRF) was performed using an M4 Tornado 2D X-ray microfluorescence spectrometer (Bruker). Three points each were analyzed for each sample; the final

data on the concentration of the elements are presented in an averaged version.

A Newport 66901 UV unit with a 66142 500 W Mercury–Xenon Lamp radiation source (Oriel Instruments) was used as the source of UV radiation. The unit operated at a power of 450 W during the synthesis.

The X-ray powder diffraction data were obtained on a D2 Phaser bench-type diffractometer (Bruker). Special low-background cells with a silicon support were used for the analysis of the samples; the analysis was performed under the rotation of the cell at a speed of 30 rpm. The X-ray diffraction patterns were recorded in a range from 5° to 90° in increments of 0.01° in the accumulation mode with a wavelength of 1.5406 Å. The time of each measurement cycle was 180 min.

The infrared (IR) spectra were recorded using CO probe molecules on a Vertex 70 IR spectrometer (Bruker) equipped with a highly sensitive detector based on mercury cadmium telluride and a Praying Mantis low-temperature reaction cell. The spectra were recorded with the resolution of 1 cm^{-1} at 64 scanning cycles. An external gas system equipped with EL-FLOW gas mass flow controller (Bronkhorst High-Tech B.V.) was used to control the flows of the gases entering the reaction chamber, namely, argon (extra pure grade, the 5.0 type, with a volume fraction of at least 99.999%), hydrogen (premium grade, the 6.0 type, ≥99.9999% volume fraction), and carbon monoxide (the 4.0 type, ≥99.99%) to create the required gas mixture. To control the pressure inside the reaction chamber (with a powdered sample placed in it), a rough pump that makes it possible to reach a pressure of up to 5×10^{-3} mbar was used. The experimental procedure was identical to that described in [14] and included two stages, namely, the activation of the sample and subsequent low-temperature adsorption/desorption of CO. At the first stage, the sample was heated to 200°C under continuous evacuation to remove water and other guest molecules and then a mixture of hydrogen (a flow rate of 5 mL/min) and argon (45 mL/min) was passed through it for 30 min to remove oxygen and possible chlorine residues. The samples were then gradually cooled to −140°C (using liquid nitrogen as a coolant) under continuous evacuation (1 h). At the second stage, the sample was purged with a CO flow (5 mL/min) for 10 min. After this, the samples were evacuated by gradually decreasing the pressure of CO inside the reaction chamber and, hence, the CO coating on the material. The IR spectra were recorded throughout the entire desorption process. The last spectrum recorded directly prior to the adsorption of CO was used as a background that was subtracted from the subsequent spectra to exclude any background signals not associated with the process of adsorption of CO.
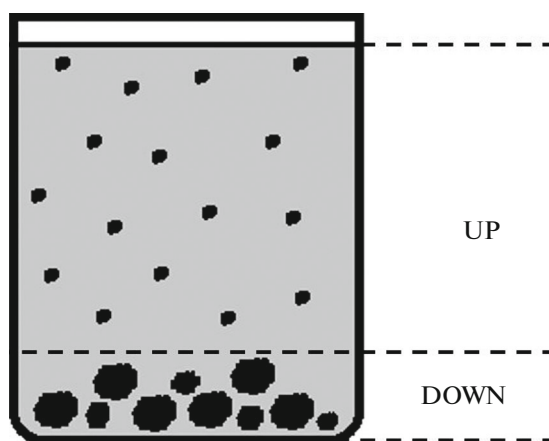

Fig. 1. The scheme of the separation of the sample to two fractions during centrifugation.

The X-ray absorption spectra were measured using an R-XAS Looper laboratory spectrometer (Rigaku). The measurements were performed in the "transmission" geometry in the absorption mode. A Ge (840) Johansson curved crystal was used as a monochromator crystal; the energy resolution at the energy of the K-edge of Pd was $\Delta E = 3.7$ eV. To measure the intensity of radiation, an ionization chamber filled with argon (300 mbar) was used before the sample and a scintillation detector was located after the sample. To measure the spectra, the powdered samples were mixed with cellulose and pressed into tablets. The measurements were performed in three passages followed by averaging.

Analysis by transmission electron microscopy (TEM) was performed on a Tecnai G2 Spirit BioTWIN microscope with an accelerating potential of 120 kV. For this, the samples were dispersed in isopropanol in an ultrasonic bath for 30 min, after which the dispersion was applied onto Formvar-coated 200 mesh Cu grids and dried in air. The obtained images were analyzed in the ImageJ software package for future construction of particle size distributions.

RESULTS

The synthesized material after centrifugation separated into two individual fractions, namely, a precipitate (the DOWN labeling) and a stable colloidal solu-

Table 1. The distribution of the main components in the UP and DOWN samples

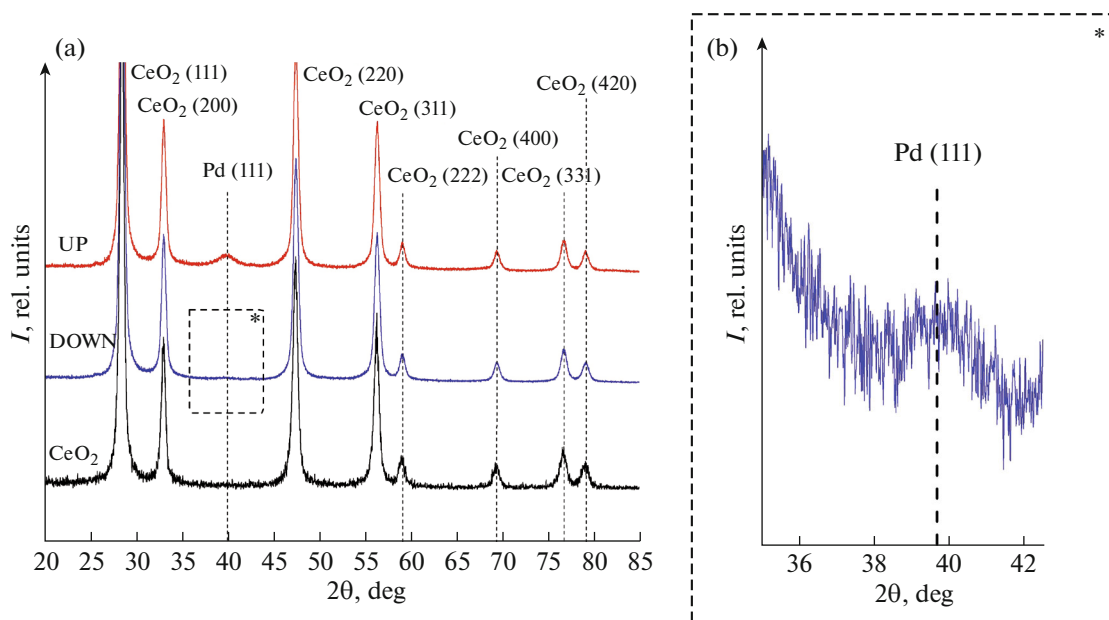| UP/DOWN	
component	weight fraction, %
Pd	7.6/4.6
CeO$_2$	92.4/95.4

Fig. 2. (Color online) (a) X-ray diffraction patterns of the UP and DOWN samples obtained in a range from 20° to 80° in increments of 0.01°; the X-ray diffraction pattern of pure CeO_2 is presented for comparison. (b) An isolated region of the X-ray diffraction pattern of the DOWN sample in a range from 35° to 42°.
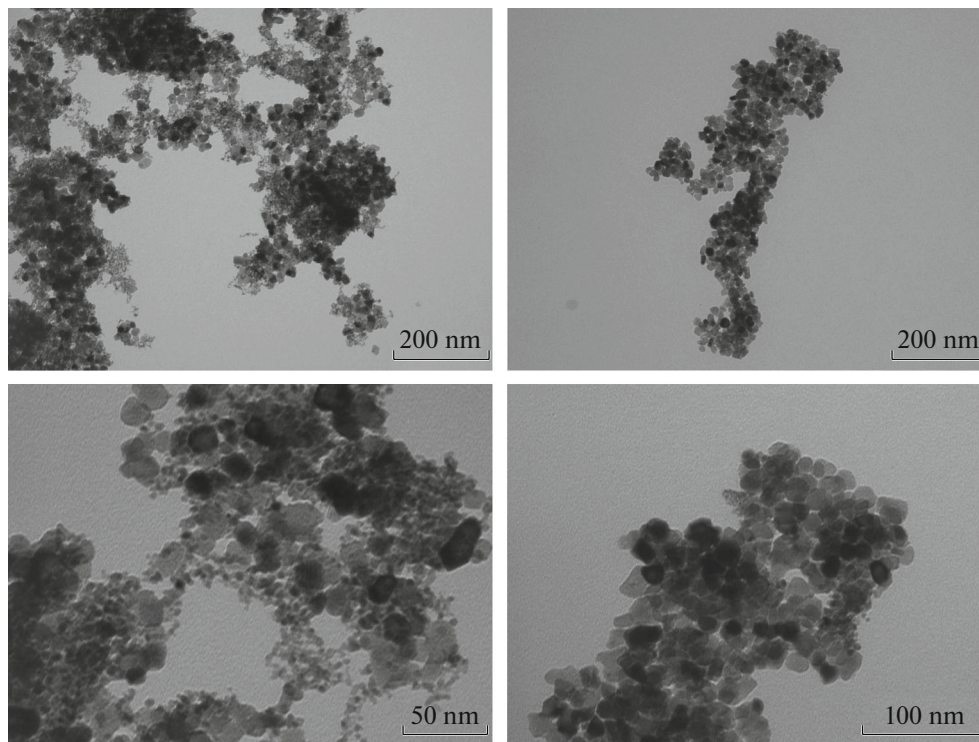

Fig. 3. TEM images of the (a, b) UP and (c, d) DOWN samples.

tion (the UP labeling). A set of procedures aimed at studying the influence of UV irradiation during the synthesis on the growth and final size of palladium nanoparticles and cerium dioxide was performed for both fractions.

XRF was used for the quantitative assessment of the weight concentration of palladium in the samples. The UP and DOWN samples were placed into a boric acid tablet. The results of the measurements are presented in Table 1. The nonuniformity of the distribution of
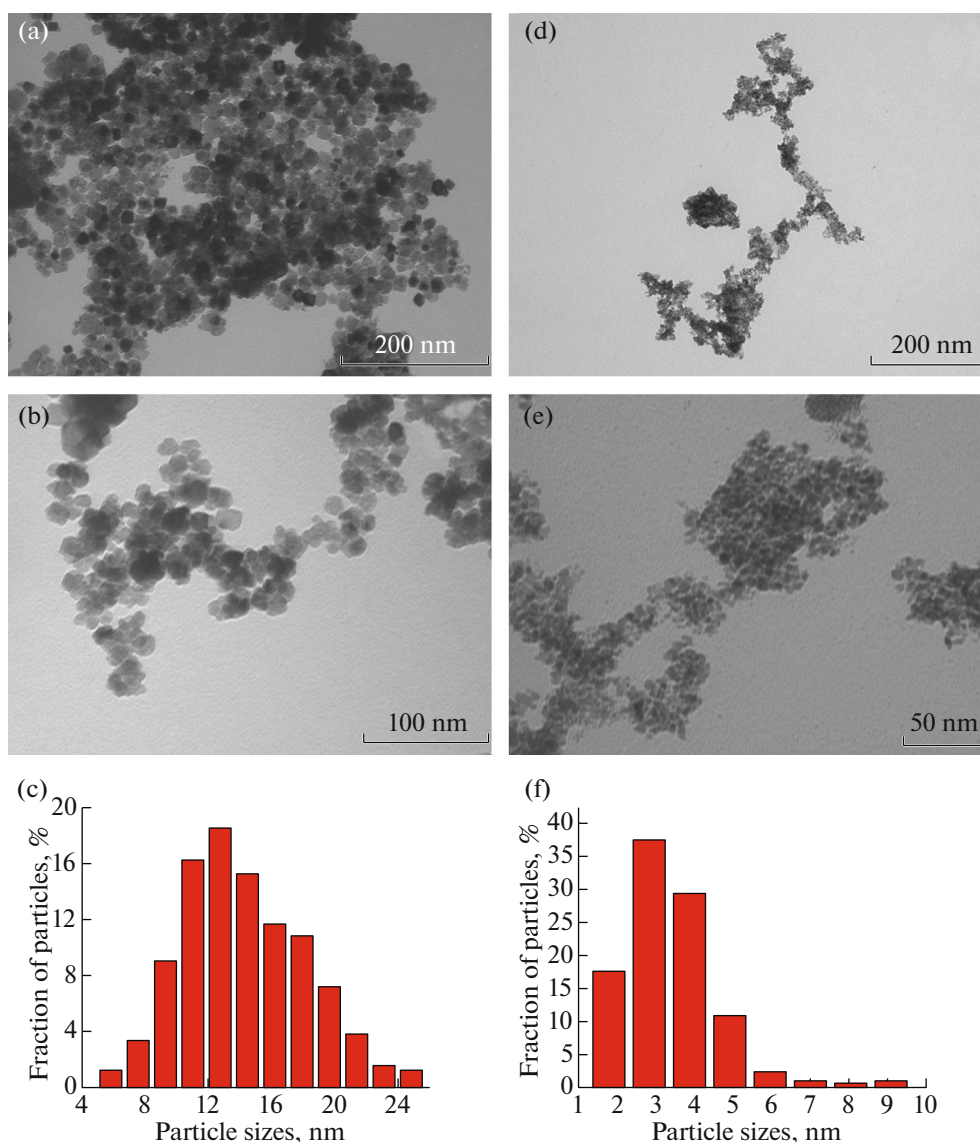
Fig. 4. (Color online) (a, b) Microimages of the CeO$_2$ sample and (c) its size distribution as well as (d, e) microimages of the Pure_Pd sample and (f) its size distribution.

palladium between the UP and DOWN fractions can be explained by the ratio of the sizes of the CeO$_2$ and Pd nanoparticles. The speed of centrifugation of 5000 rpm was insufficient for the precipitation of the major part of ultrasmall Pd nanoparticles, thus, the DOWN fraction consisted of relatively large agglomerates of CeO$_2$ particles partially coated with Pd, while the UP sample consisted of well-dispersed CeO$_2$ nanoparticles uniformly coated with Pd. Therefore, the concentration of Pd nanoparticles in the DOWN sample was lower than that in the UP sample.

The results of characterization by X-ray powder diffraction are presented in Fig. 2a. The X-ray diffraction patterns of the UP and DOWN samples demonstrate the same numbers and positions of the peaks

assigned to the phase of cerium dioxide. Here, differences are present in the data concerning Pd, thus, a pronounced peak of Pd(111) was present in the UP sample, while the intensity of this peak was at the noise level in the DOWN sample (Fig. 2b). The difference in the intensity can be explained by both the different concentrations of Pd and their smaller size. In the case of the DOWN sample, the agglomeration of the particles could partially block the possibilities for their growth, thus complicating the penetration of the UV radiation. No presence of the phase of PdO was detected based on the data of X-ray powder diffraction.

The UP and DOWN samples were characterized by TEM (Fig. 3); however, the data did not allow accurate identification of the particles in the microim-
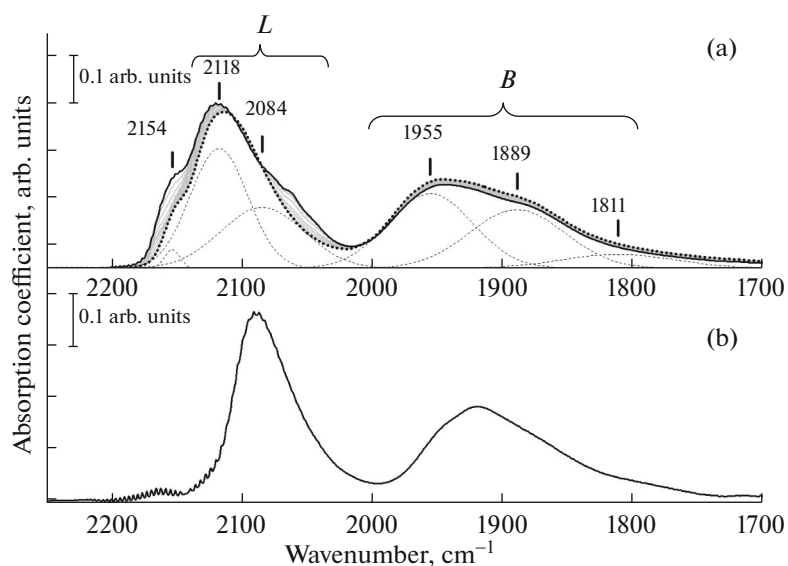
Fig. 5. (a) The IR spectra of the UP sample measured during the desorption of CO at −140°C preliminarily reduced at 200°C in a 5% H_2/Ar mixture. The spectrum measured at the highest coating by CO (P_{CO} = 4 mbar) is highlighted by a solid black bold line; the series of spectra obtained upon decreasing the coating by CO is shown in grey; and the spectrum after continuous evacuation for 10 min (P_{CO} = 5 × 10^{-3} mbar) is highlighted by a dotted line. The dashed line shows the results of the approximation of the last of the above spectra by the Gauss function. (b) IR spectrum of the DOWN sample measured after the adsorption of CO at the highest coating by CO (P_{CO} = 6.4 mbar).

ages due to the small differences in the contrast range of the cerium and palladium atoms (the charge number of Ce is 58, while that of Pd is 46). Moreover, the resolution of these microimages is insufficient to make unambiguous conclusions about the sizes and shape of the palladium nanoparticles. Nevertheless, it is seen from the analysis of the images that the substrate is a combination of small CeO_2 nanoparticles rather than larger micrometer-scale particles in both UP sample and the DOWN sample. For comparison, palladium nanoparticles were synthesized according to a similar procedure [23] that differs by the absence of cerium dioxide nanoparticles in the system (a control sample denoted as Pure_Pd). Pure cerium dioxide (CeO_2) was also used as a reference sample. The particle size distribution was estimated for the samples of pure CeO_2 and the reference sample of Pure_Pd from the obtained microimages (300 nanoparticles were analyzed for each sample, Fig. 4). In the CeO_2 sample the nanoparticles are characterized by dispersion in the range of 6–26 nm with a predominant fraction of 14 nm. It is seen from the analysis of the microimages that CeO_2 in the UP and DOWN samples has no noticeable differences in size when compared to CeO_2 that was individually synthesized. The size of the obtained nanoparticles can be judged by the results of the analysis of the TEM images of Pure_Pd (1.5–9.5 nm). However, comparison of the UP and DOWN samples is challenging. The sizes of the palladium nanoparticles in the above samples can only be indirectly estimated using different procedures.

Due to necessity of drying samples for carrying out the TEM measurement and the formation of large conglomerates of the catalyst particles that inevitably accompanies this process it is impossible to confirm or reject the hypothesis about the difference of the UP and DOWN samples with respect to the size of the agglomerates in the solution based on the resulting microimages; special liquid-type cells should be used for this.

IR spectroscopy in combination with the use of CO probe molecules made it possible to detect the presence of palladium nanoparticles for the UP sample, which manifested itself by the presence of two bands in a range of 2150−1700 cm^{-1} (Fig. 5a). A similar picture was observed for the DOWN sample (Fig. 5b). In particular, a group of absorption bands with a maximum at 2121 cm^{-1} was observed in this region, which underwent a barely noticeable red shift to 2118 cm^{-1} under evacuation. A shoulder in the low-frequency region was observed for this band which, as was found by approximation of the spectrum with the lowest coating, was associated with another absorption peak with a maximum near 2084 cm^{-1}. As well, a low-intensity peak that made a contribution to this absorption band with a maximum at approximately 2154 cm^{-1} was detected in the high-frequency region. This peak was assigned to the adsorption of CO on the material of the substrate, which is in agreement with the observations of some authors who assign this peak either to the case of adsorption on Ce^{3+} [32−34] or to adsorption on the
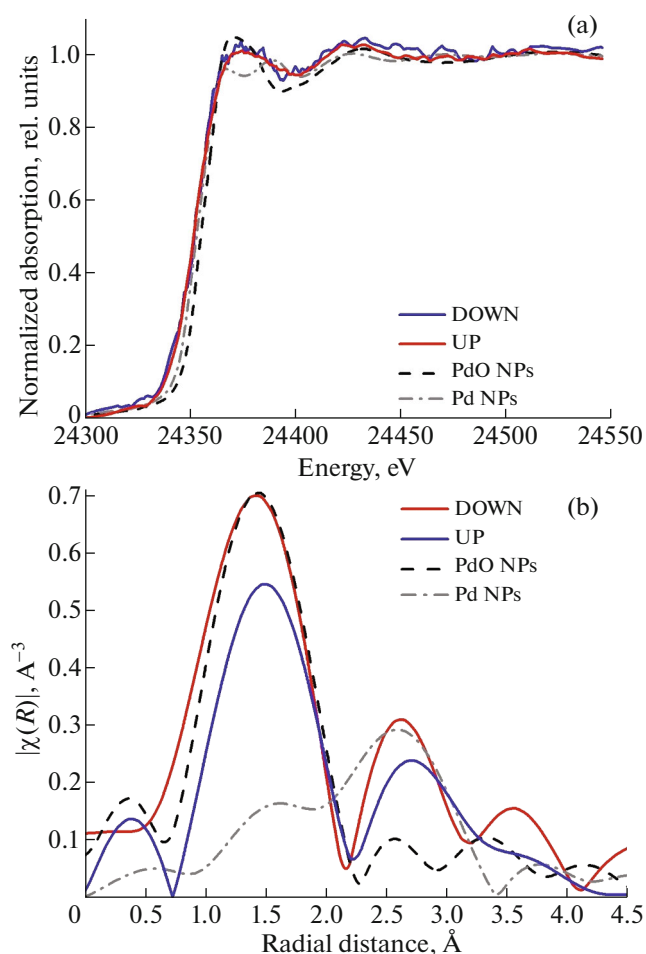
Fig. 6. (Color online) (a) X-ray absorption spectra beyond the K-edge of Pd for the UP and DOWN samples in comparison with the spectra of palladium nanoparticles and palladium oxide. (b) Results of the qualitative Fourier analysis of the X-ray absorption spectra in the XAFS region beyond the K-edge of Pd for the UP and DOWN samples, palladium nanoparticles, and palladium oxide.

coordinatively unsaturated Ce^{4+} sites [35−37]. No adsorption of CO on Pd^{2+} ions, which manifests itself in the form of an adsorption band in the region of 2170 cm^{-1} according to the data of [38, 39], was detected; this gives evidence of the full reduction of Pd during the mode of activation in hydrogen.

The high-frequency peak can be assigned to CO molecules that are linearly adsorbed on highly dispersed but noncrystalline palladium particles [40]. The low-frequency component is apparently associated with the formation of linear carbonyls on the defects (corners, edges, and steps) of Pd nanoparticles. Such a behavior during evacuation is in agreement with the fact that CO is more strongly bound to the defects of palladium [41], which leads to a greater shift in comparison with the frequency of vibrations of CO in the gas phase (2143 cm^{-1}). This group of peaks is denoted by the symbol *L* in Fig. 5.

Another group (denoted by the symbol *B* in Fig. 5) that consists of at least three peaks was observed in a range from 2000 to approximately 1750 cm^{-1}. It was found by approximation that the maxima of these absorption bands are located at approximately 1955, 1889, and 1811 cm^{-1} at the minimum pressure of CO (after 10 min of evacuation and a pressure of 5 × 10^{-3} mbar). They can be assigned to the case of formation of so-called bridging carbonyls on the defects, as well as on two or three Pd(111) atoms. This result is in agreement with the results of [42].

As shown in [43], a conclusion about the size of nanoparticles can be made based on the ratio of the areas under the peaks assigned to the linear and bridging carbonyls because an increase in the extended sections leads to growth in the number of bridging carbonyls that are formed (the *B* group grows), while, on the other hand, the reduction in the sizes of nanoparticles leads to the predominance of linearly adsorbed molecules (the *L* group grows). The obtained *B*/*L* ratio of the areas was 1.12, which is close to the results obtained under identical conditions in [14], where the *B*/*L* ratio was 1.4 for the nanoparticles with a size of approximately 2.1 nm. This provides evidence of a significant fraction of ultrasmall Pd nanoparticles with a size of less than 2 nm in the UP sample. Comparable ratios of the areas were also observed for the DOWN sample (Fig. 5b); however, their detailed assessment was not performed. The influence of the substrate on the size of the palladium nanoparticles, which were substantially smaller in comparison with those synthesized without a substrate (Pure_Pd), can be explained by the formation of a large number of crystallite nuclei on the active surface of cerium dioxide due to the high degree of adsorption of $[Pd(C_2O_4)_2]^{2-}$ ions.

Figure 6a presents the X-ray absorption spectra near the K-edge of Pd for the UP and DOWN samples in comparison with the spectra of palladium nanoparticles and palladium oxide obtained during the measurements at the facilities of the European Synchrotron Radiation Facility, (ESRF, Grenoble, France) as part of the studies in [44]. The energy calibration of the spectra was performed based on the spectra of reference palladium compounds.

Comparison of the X-ray absorption spectra (XAFS) beyond the K-edge of Pd (Fig. 6a) shows that although the position of the edge for the samples is similar to that for metal nanoparticles with respect to energy, pronounced characteristic features inherent to palladium in an oxygen environment are present in the spectrum profile in the near-edge region that is sensitive to the local electronic structure and lengths and angles of the chemical bond of the absorbing atom. This may be associated with the oxidation of palladium on the surface of the nanoparticles in an air atmosphere.

Figure 6b presents the results of qualitative assessment of the radial distribution of the atoms around Pd

obtained from the experimental X-ray absorption spectra by the k^2-weighted Fourier transform without phase correction. The distribution for the UP and DOWN samples contains, in addition to the peaks that are characteristic of metal nanoparticles, an intensive peak at 1.45 Å that indicates the presence of oxygen in the environment of Pd. Unfortunately, the quality of the laboratory spectra obtained for the samples does not allow full performance of an analysis of the extended X-ray absorption fine structure and quantitative analysis of the coordination numbers of Pd. Because of this, it is difficult to answer the question about what produces this signal and at what proportion: oxygen in the CeO_2 substrate or palladium oxide present on the surface of the nanoparticles.

CONCLUSIONS

Successful reduction of a complex precursor of palladium(II) on a cerium(IV) oxide substrate by UV radiation has been performed.

The data obtained by XRF, TEM, X-ray powder diffraction, XAFS, and IR spectroscopy with CO probe molecules made it possible to determine the structure and phase composition of the studied substance, as well as to approximately estimate the size of the Pd nanoparticles.

The analysis of X-ray powder diffraction has shown the presence of a peak characteristic for the phase of palladium in the UP sample. In addition, the analysis data indicate that the concentration of palladium is higher in the UP sample when compared to the DOWN sample. This conclusion is confirmed by the data of XRF, which show a higher weight fraction of palladium in the UP sample (7.6%) than in the DOWN sample (4.6%).

An assumption has been made about the formation of a significant fraction of large particle agglomerates during the synthesis that were deposited upon centrifugation (the DOWN sample), which blocked the growth of a significant fraction of Pd nanoparticles due to the shielding of the UV radiation. It has been found that the DOWN sample consists of agglomerates of CeO_2 nanoparticles rather than of micron-scale particles.

The analysis of the IR spectra with the use of CO probe molecules and ratio of the areas under the peaks associated with the formation of bridging and linear carbonyls confirmed the presence of ultrasmall (smaller than 2 nm) palladium particles. This size is significantly smaller than that observed for the Pure_Pd reference sample where CeO_2 was not used as the substrate.

The analysis of the X-ray absorption spectra in the XAFS region beyond the K-edge of Pd showed the presence of a certain fraction of palladium atoms in the oxide phase. This was confirmed by the results of the qualitative Fourier analysis of the experimental X-ray absorption spectra, which provide evidence of the presence of oxygen in the environment of Pd. The appearance of the oxide phase can be determined by both the high reactivity of nanosized Pd, which is readily oxidized in air at room temperature, and the relative readiness of the $Ce^{4+} \rightleftarrows Ce^{3+}$ oxidation–reduction transitions (1.66 V), which allows CeO_2 release of catalytically active forms of oxygen that oxidize palladium atoms at the site of their contact with cerium dioxide.

ADDITIONAL INFORMATION

M.V. Kirichkov, engineer, ORCID: https://orcid.org/0000-0002-4318-2727

V.A. Polyakov, engineer, ORCID: https://orcid.org/0000-0002-6774-8983

A.A. Tereshchenko, engineer, ORCID: https://orcid.org/0000-0001-5102-6743

V.V. Shapovalov, research engineer, ORCID: https://orcid.org/0000-0001-6361-0437

A.A. Guda, head of a research laboratory, ORCID: https://orcid.org/0000-0002-6941-4987

A.V. Soldatov, director of Smart Materials Research Institute, ORCID: https://orcid.org/0000-0001-8411-0546

REFERENCES

1. M. Z. Atashbar and S. Singamaneni, Sens. Actuators, B **111−112**, 13 (2005).
2. C. -Y. Liu and A. J. Bard, Nature (London, U.K.) **418**, 162 (2002).
3. V. K. Markova, J. P. Philbin, W. Zhao, et al., ACS Catal. **8**, 5675 (2018).
4. Y. Li, E. Boone, and A. M. El-Sayed, Langmuir **18**, 4921 (2002).
5. J. C. Garcia-Martinez, R. Lezutekong, and R. M. Crooks, J. Am. Chem. Soc. **127**, 5097 (2005).
6. C. Du, Y. Guo, Y. Guo, et al., J. Mater. Chem. A **3**, 23230 (2015).
7. M. Cargnello, T. Montini, S. Polizzi, et al., Dalton Trans. **39**, 2122 (2010).
8. H. Dai, H.-B. Dai, Y.-J. Zhong, et al., Int. J. Hydrogen Energy **42**, 5684 (2017).
9. A.-G. Boudjahem, A. Redjel, and T. Mokrane, J. Ind. Eng. Chem. **18**, 303 (2012).
10. T. Feng, R. Tang, N. Shang, et al., Appl. Organomet. Chem. **31**, 3889 (2017).
11. F. Fievet, J. P. Lagier, and B. Blin, Solid State Ionics **32−33,** 198 (1989).
12. H. Li, G. Sun, Q. Jiang, et al., Electrochem. Commun. **9**, 1410 (2007).

13. C. Coutanceau, S. Baranton, and T. W. Napporn, Deliv. Nanopart. **19**, 403 (2012).
https://doi.org/10.5772/18179

14. A. Tereshchenko, V. Polyakov, A. Guda, et al., Catalysts **9**, 385 (2019).

15. S. Somboonthanakij, O. Mekasuwandumrong, J. Panpranot, et al., Catal. Lett. **119**, 346 (2007).

16. R. Strobel, J. Catal. **222**, 307 (2004).

17. S. Chaudhary, P. Sharma, D. Singh, et al., ACS Sustainable Chem. Eng. **5**, 6803 (2017).

18. J. Xu, L. Li, and G. Li, J. Dispers. Sci. Technol. **29**, 1072 (2008).

19. A. B. Jorge, Y. Sakatani, C. Boissière, et al., J. Mater. Chem. **22**, 3220 (2012).

20. M. Sortland, J. Hotalen, R. D. Re, et al., J. Micro/Nanolithogr. MEMS. MOEMS **14**, 043511 (2015).

21. M. Grzelczak and L. M. Liz-Marzán, Chem. Soc. Rev. **43**, 2089 (2014).

22. T. Bian, L. Shang, H. Yu, et al., Adv. Mater. **26**, 5613 (2014).

23. S. Navaladian, B. Viswanathan, T. K. Varadarajan, and R. P. Viswanath, Nanoscale Res. Lett. **4**, 181 (2008).

24. N. Ullah, M. Imran, K. Liang, et al., Nanoscale **9**, 13800 (2017).

25. P. Liu, J. Chen, and N. Zheng, Chin. J. Catal. **38**, 1574 (2017).

26. H. Khojasteh, M. Salavati-Niasari, A. Abbasi, et al., J. Mater. Sci.: Mater. Electron. **27**, 1261 (2015).

27. X. Song, Q. Shi, H. Wang, et al., Appl. Catal., B **203**, 442 (2017).

28. M. Martis, W. Meicheng, K. Mori, and H. Yamashita, Catal. Today **235**, 98 (2014).

29. M. Yuasa, T. Kida, and K. Shimanoe, ACS Appl. Mater. Interfaces **4**, 4231 (2012).

30. P. Lu, B. Qiao, N. Lu, et al., Adv. Funct. Mater. **25**, 4153 (2015).

31. R. Pilný, P. Lubal, and L. Elding, Dalton Trans. **43**, 12243 (2014).

32. A. Badri, C. Binet, and J.-C. Lavalley, J. Chem. Soc., Faraday Trans. **92**, 1603 (1996).

33. K. Mudiyanselage, H. Y. Kim, S. D. Senanayake, et al., Phys. Chem. Chem. Phys. **15**, 15856 (2013).

34. S. Chen, T. Cao, Y. Gao, et al., J. Phys. Chem. C **120**, 21472 (2016).

35. F. Bozon-Verduraz and A. Bensalem, J. Chem. Soc., Faraday Trans. **90**, 653 (1994).

36. C. Li, Y. Sakata, T. Arai, et al., J. Chem. Soc., Faraday Trans. 1 **95**, 929 (1989).

37. C. Binet, M. Daturi, and J.-C. Lavalley, Catal. Today **50**, 207 (1999).

38. X. Wang, G. Wu, N. Guan, and L. Li, Appl. Catal., B **115−116,** 7 (2012).

39. T. Baidya, P. Bera, B. D. Mukri, et al., J. Catal. **303**, 117 (2013).

40. F. Gregorio, L. Bisson, T. Armaroli, et al., Appl. Catal., A **352**, 50 (2009).

41. I. V. Yudanov, R. Sahnoun, K. M. Neyman, et al., J. Phys. Chem. B **107**, 255 (2003).

42. Q. Fan, S. He, L. Hao, et al., Sci. Rep. **7**, 42172 (2017).

43. L. L. Sheu, Z. Karpinski, and W. M. H. Sachtler, J. Phys. Chem. **93**, 4890 (1989).

44. A. L. Bugaev, A. A. Guda, I. A. Pankin, et al., Catal. Today **336**, 40 (2019).

Translated by E. Boltukhina